Broadband Cavity-Enhanced Detection of Magnetic Field Effects in Chemical Models of a Cryptochrome Magnetoreceptor

ARTICLE *in* THE JOURNAL OF PHYSICAL CHEMISTRY B · MARCH 2014

Impact Factor: 3.3 · DOI: 10.1021/jp500732u · Source: PubMed

THE JOURNAL OF PHYSICAL CHEMISTRY B

Article

pubs.acs.org/JPCB

Broadband Cavity-Enhanced Detection of Magnetic Field Effects in Chemical Models of a Cryptochrome Magnetoreceptor

Simon R. T. Neil,[†] Jing Li,[†] Dean M. W. Sheppard,[†] Jonathan Storey,[‡] Kiminori Maeda,[‡] Kevin B. Henbest,[‡] P. J. Hore,[†] Christiane R. Timmel,*[,‡] and Stuart R. Mackenzie*[,†]

[†]Department of Chemistry, Physical & Theoretical Chemistry Laboratory, University of Oxford, Oxford, OX1 3QZ, United Kingdom

[‡]Department of Chemistry, Inorganic Chemistry Laboratory, University of Oxford, Oxford, OX1 3QR, United Kingdom

ABSTRACT: Broadband cavity-enhanced absorption spectroscopy (BBCEAS) is shown to be a sensitive method for the detection of magnetic field effects (MFEs) in two flavin-based chemical reactions which are simple models for cryptochrome magnetoreceptors. The advantages of optical cavity-based detection and (pseudo-white-light) supercontinuum radiation have been combined to provide full spectral coverage across the whole of the visible spectrum ($425 < \lambda < 700$ nm). This region covers the absorbance spectra of flavin mononucleotide (FMN) and flavin adenine dinucleotide (FAD) as well as their photogenerated radicals. To illustrate the power of this technique, BBCEAS has been used to record the spectral dependence of MFEs for photoinduced radical pairs formed in the intermolecular reaction of FMN with lysozyme and the intramolecular photochemistry of FAD. These reactions have been chosen for their photochemical similarities to cryptochrome proteins which have been proposed as key to the magnetic compass sense of many animals including birds. In experiments performed using low protein concentrations (10 μM) and 1 mm optical path-lengths, absorbance changes as small as 1×10^{-7} (representing <0.1% MFEs) have been detected with good signal-to-noise offering the prospect of sensitive MFE detection in cryptochrome.

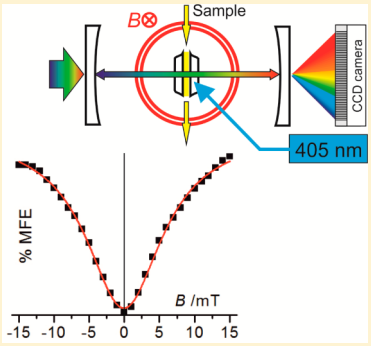

I. INTRODUCTION

The study of magnetic field effects (MFEs) on spin-correlated radical pairs (RPs) has assumed new prominence in recent years with the suggestion that such effects, resulting from the differing fates or reaction kinetics of singlet and triplet states, may lie at the heart of the compass magnetoreception mechanism in animals such as migratory birds.[1] Much of this activity has been driven by the discovery of the cryptochrome family of blue-light receptor proteins, some of whose members appear to possess the necessary prerequisites for exhibiting MFEs within the framework of the radical pair mechanism.[2−4] Indeed, an MFE in a plant cryptochrome (from *Arabidopsis thaliana*) was recently reported in vitro,[5] and significant MFEs have also been observed in photoinitiated electron transfer reactions of a closely related DNA photolyase.[6]

Short-lived radical pairs, the key to MFEs, have been studied intensively for several decades.[7−10] Radical pairs may be produced by a variety of means including pulse radiolysis and thermal activation, but, most commonly, are photogenerated by electronic excitation of a precursor. This is typically followed by rapid electron transfer with conservation of spin angular momentum. Sensitivity to an externally applied magnetic field arises from the ability of the field to influence the efficiency with which the singlet and triplet states of the radical pair interconvert. If spin-selective recombination from the singlet and triplet states occurs at different rates, and/or results in different products, the reaction kinetics and yields may exhibit magnetosensitivity. In 2008, Maeda et al. demonstrated, using a chemical model system, that even magnetic fields as weak as that of the Earth, ca. 50 μT, can influence the recombination reactions of radical pair intermediates.[11]

Traditional techniques of choice for the study of MFEs mainly involve optical spectroscopy. Luminescence methods have been widely used in combination with photoexcitation.[7] Optical absorption approaches, such as laser flash photolysis and transient absorption spectroscopy, have also been employed. Although more generally applicable, they typically suffer from inferior sensitivity compared with emission techniques and require comparatively large sample volumes and high concentrations. To date, these requirements have hindered their applicability to real biological samples.

In recent years we have developed a suite of optical cavity-based techniques with the aim of detecting MFEs in solution with higher sensitivity than commonly achieved using traditional single-pass techniques.[6,12] Neil et al. demonstrated the use of field modulation in combination with diode-laser cavity-enhanced absorption in detecting MFEs on the reaction of thionine with 1,4-diazabicyclo[2.2.2]octane (DABCO).[12] Subsequently, Maeda et al. used a pump−probe technique including cavity ring-down detection[13,14] to study time-resolved MFEs.[6] Ultimately, it is hoped that such techniques will provide the step change in sensitivity required to study precious biological samples despite the associated problems of small volumes and low concentrations. To date, however, these

Received: January 21, 2014
Revised: March 19, 2014
Published: March 21, 2014

approaches have been restricted to single-wavelength measurements. In turn, this limits their applicability to systems in which a measurable absorbance difference is produced at a wavelength for which a suitable light source (e.g., a diode laser) is available. In simple chemical systems, this may be readily achieved. However, in the case of complex biological molecules, such as cryptochromes, the possibilities exist for different species (such as the flavin chromophore) to be present in various oxidation or protonation states, each of which has its own characteristic absorbance spectrum.[15]

Here, we report on the application of broadband cavity-enhanced absorption spectroscopy (BBCEAS) employing supercontinuum radiation for the simultaneous recording of MFEs across the whole of the visible spectrum from 425 to 700 nm. This method couples the sensitivity gains afforded by multipassing within high finesse optical cavities with the multiplex advantage of a truly broadband technique. As this is the first application of BBCEAS to MFE detection, we describe in some detail the construction, optimization and calibration of the instrument used and its detection limits.

II. EXPERIMENTAL SECTION

A. FMN | Lys and FAD Photochemical Reactions. For the proof-of-principle measurements described here, the reaction of flavin mononucleotide with lysozyme (FMN | Lys) has been used.[16] This system is a well understood chemical model with many photochemical features in common with the FAD | Trp (flavin adenine dinucleotide | tryptophan) radical pair generated by blue-light excitation of cryptochrome and photolyase proteins.[10] The same system was also the subject of our previous cavity ring-down spectroscopic[6] study permitting comparison of the current broadband, continuous-wave experiment with the earlier single-wavelength, pump−probe measurements.

The FMN | Lys photochemical reaction is shown in Scheme 1. Photoexcitation of the flavin ground state at 405 nm generates the excited singlet state ^{1}FMN*. This undergoes intersystem crossing (ISC) on the nanosecond time scale to yield ^{3}FMN*.[17] In turn, the long-lived ^{3}FMN* state is reduced by electron transfer (ET) from a tryptophan residue on the surface of the lysozyme molecule, with conservation of total spin angular momentum, to form a triplet-born radical pair, $^3[FMN^{-\bullet}\ Trp(H)^{+\bullet}]$. This triplet-born radical pair is unreactive (recombination to the ground state being spin-forbidden), and either it undergoes singlet−triplet mixing or the radicals diffuse apart to form free radicals. Crucially, the efficiency of the former process, which is driven by the interaction of electron spins with neighboring magnetic nuclei (i.e., hyperfine interactions), is sensitive to the applied magnetic field. As the singlet radical pair, $^1[FMN^{-\bullet}\ Trp(H)^{+\bullet}]$, has an additional decay pathway available (recombination to the ground state), this endows the total free radical yield with a measurable magnetic field dependence.

Scheme 1. Photochemical Reaction Scheme for the FMN | Lys System[a]

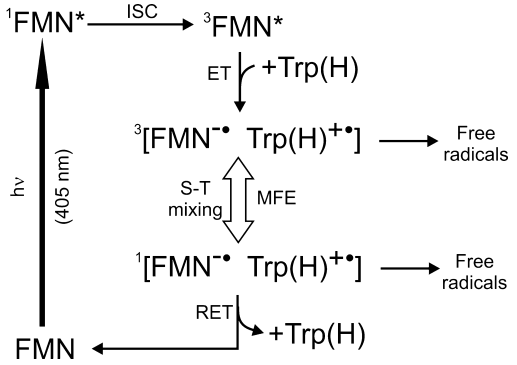

[a]Photoexcitation of FMN at 405 nm leads to formation of a triplet-born radical pair. ISC: intersystem crossing. ET: electron transfer. In this state the pair can either diffuse apart or undergo singlet−triplet mixing. The singlet radical pair can return to the ground state species by reverse electron transfer (RET).

The FMN | Lys reaction, while similar to that proposed as the source of magnetosensitivity in cryptochromes, differs in (at least) one important respect. In cryptochromes, the electron transfer leading to the spin-correlated radical pair is known to be an *intra*molecular process in which the reduction of the flavin cofactor occurs by rapid electron transfer along a triad of tryptophan residues, finally resulting in the formation of a $[FAD^{-\bullet}\ Trp(H)^{+\bullet}]$ radical pair.[1,10,18] In order to study such intramolecular radical pair production, we have further applied the BBCEAS technique to detect MFEs in free FAD in the absence of additional electron donors. The photochemistry of FAD (see Scheme 2) bears closer resemblance to cryptochrome than the FMN | Lys reaction in that (i) FAD is the flavin derivative found in cryptochromes and (ii) the radical pair formation occurs via intramolecular electron and proton transfer processes. In other respects, the FAD reaction is similar to FMN | Lys with a triplet-born radical pair whose conversion to the singlet state is magnetic field-dependent. Free radical species can be generated by bimolecular reaction of the molecular triplet state, but its short lifetime leads to much reduced steady-state free radical concentrations compared to FMN | Lys. The radical lifetime in FAD, at 1−10 μs, is also significantly shorter than for the FMN | Lys reaction.[10,19,20]

Scheme 2. Photochemical Scheme for the FAD (= F-AH$_2^+$) Reaction at pH 2[a]

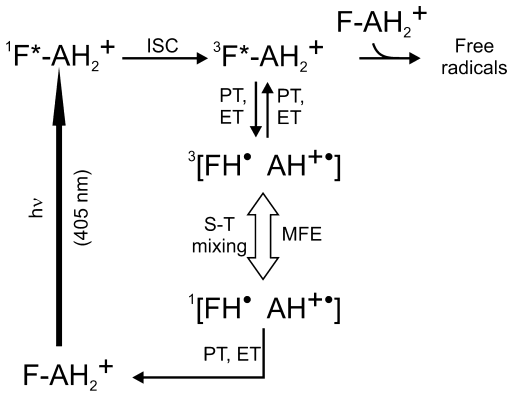

[a]In contrast to the FMN | Lys reaction, radical pair formation occurs via (reversible) intramolecular proton and electron transfer steps (PT, ET) between the flavin (F) and adenine (A) groups.

B. Materials. Hen egg-white lysozyme (Sigma-Aldrich) and the sodium salt of FMN (Sigma-Aldrich) were used without further purification. Solutions were made up to 10 μM FMN and 500 μM lysozyme using ultrapure water (Milli-Q, resistivity >18.2 MΩ cm).

dx.doi.org/10.1021/jp500732u | J. Phys. Chem. B 2014, 118, 4177−4184

The disodium salt of FAD (Sigma-Aldrich) was used without further purification. Aqueous solutions of FAD were diluted to 10 μM concentrations using aqueous citrate buffer solution ($Na_2HPO_4 \cdot 10H_2O$/citric acid monohydrate) at pH 2.2. The low pH ensures protonation of the flavin, which prevents flavin-adenine ring stacking in the ground state.[21]

C. Broadband Cavity-Enhanced Absorption Spectroscopy. Our earlier cavity-enhanced approaches to MFE detection[6,12] were limited to single-wavelength measurements and required non-overlapping absorption features of different species. Here, we present a continuous-wave broadband variant of CEAS capable of simultaneous measurement of MFEs across the full visible spectrum.

CEAS takes advantage of multiple passes of light trapped within a high finesse optical cavity formed by two highly reflective mirrors.[22] Light is continuously pumped into the cavity and the light circulating reaches a steady-state level dependent on the incident intensity and the absorption and scattering losses within the cavity. It can be shown that the per-pass absorbance, A, of a sample within the cavity is given in terms of the ratio of the light intensity transmitted by the cavity in the presence of the absorber, I, to that transmitted by an empty cavity, I_0, by[22]

$$A \times \ln 10 \times \mathrm{CEF} = \left(\frac{I_0}{I} - 1\right) \quad (1)$$

in which ln 10 (= 2.3026) converts the measured values to the conventional condensed phase decadic ($\log_{10}$) scale. CEF is the cavity enhancement factor which provides a measure of the effective increase in path-length over a single-pass experiment. It is often represented as $(1 - R_{\mathrm{eff}})^{-1}$ in which R_{eff} is an effective mirror reflectivity including all background (non-absorptive) losses intrinsic to the cavity.

Although it is conceptually appealing to consider the sensitivity improvements in CEAS as arising from the increased optical path-length afforded by multipassing, Ouyang and Jones have recently pointed out that the total number of photons absorbed by the sample is the same as in a well-designed single-pass experiment, and that the improvement in signal-to-noise results from noise suppression.[23]

Developed originally for gas-phase spectroscopy, CEAS has found recent application in both the bulk condensed phase (where Ruth,[24] Islam,[25−28] and Kaminski[28,29] have been prominent proponents) and, via evanescent waves, at interfaces.[30−33]

D. BBCEAS−MFE Instrument. The instrument used in these studies is shown schematically in Figure 1. At the heart of the experiment sits a 1 mm optical path-length sample flow cell (Hellma 165−1.0−40 or Starna 45/Q). This cell was selected for the high optical quality of its windows, which is crucial for cavity-based experiments. The cell is surrounded by a pair of magnetic field coils arranged as a Helmholtz pair and used to apply homogeneous magnetic fields in the region of the cell, perpendicular to the optical axis. No attempt is made to shield the instrument from the Earth's magnetic field (ca. 0.05 mT in the UK, inclined at 66° to the horizontal). Although this field is small compared with those employed in these studies, we deliberately sweep the strength of the applied field between equal and opposite extremes ($\pm B_{\mathrm{max}}$) to minimize the risk of asymmetry in the measurements.

The cell is mounted at the center of a simple optical cavity formed from two broadband-coated, highly reflective mirrors

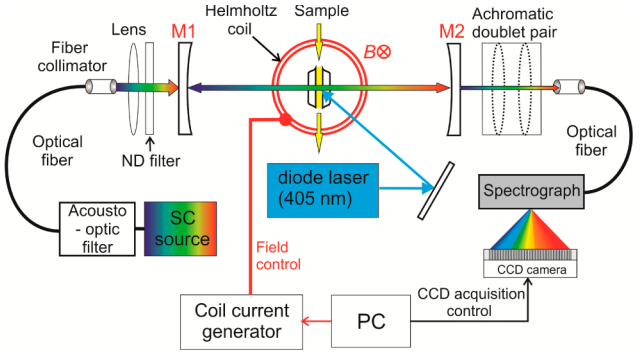

Figure 1. BBCEAS instrument used for magnetic field effect studies. The system comprises a white-light (supercontinuum) radiation source, an optical cavity with intracavity cell surrounded by Helmholtz coils, a grating spectrometer, and a CCD array for detection.

(M1 and M2 in Figure 1, Layertec $R_{400-800\ \mathrm{nm}} > 0.9993$, radius of curvature = 0.5 or 1.0 m) mounted ca. 0.20 m apart. The cell sits on a goniometer rotation stage, which enables the optical axis of the cell to be arranged collinearly with that of the optical cavity. Radicals are generated within the cell by continuous photoexcitation at 405 nm using a continuous-wave diode laser (350 mW, Power Technology).

The broadband (white-light) probe beam is provided in these studies by a supercontinuum radiation (SCR) source. The use of SCR sources for truly broadband CEAS has been pioneered by Kaminski and co-workers.[34,35] In many respects, SCR sources are less than ideal for sensitive absorbance measurements, as they suffer from spectral power fluctuations inherent in the nonlinear processes involved in supercontinuum generation. For future use, various (more stable) light emitting diode-based alternatives are being developed.[25,27] However, the collimated, laser-like output of the SCR source greatly aids in coupling light into an optical cavity and, where direct comparisons have been made, the performance of the SCR source proved superior.[33] In these studies, two SCR sources with similar characteristics (NKT Koheras SuperK Power Blue and Fianium SC400−4) have been used. In each case, the output is spectrally filtered to remove the infrared component ($\lambda > 800$ nm) with the remaining visible output (425−800 nm, up to 400 mW total power) delivered to the cavity via an optical fiber. For the purposes of these studies the supercontinuum radiation (generated by pumping a photonic crystal fiber with a high, e.g., 80 MHz, repetition rate picosecond laser) is treated as quasi-continuous.

The output from the cavity exiting via mirror M2 is focused using an achromatic doublet pair into a further optical fiber and coupled into a grating spectrometer (Andor, Shamrock Spectrograph, 150 line/mm grating with 500 nm blaze), which disperses the light onto a charge-coupled device (CCD) array (Andor Newton Spectroscopy Camera, 1024 × 255 pixel). The monochromator entrance slits were set to 100 μm to increase the transmission. This results in a spectral resolution of ca. 5 nm, which is narrower than the broad spectral features of interest. For all experiments, acquisition times of 40−50 ms were typically used; Allan variance measurements indicated that this gave an optimal compromise between short-term intensity fluctuations and longer-term drift in the SCR sources.

The whole instrument, including light sources and magnetic fields, is controlled by custom-written LabVIEW and/or C++ programs.

dx.doi.org/10.1021/jp500732u | J. Phys. Chem. B 2014, 118, 4177−4184

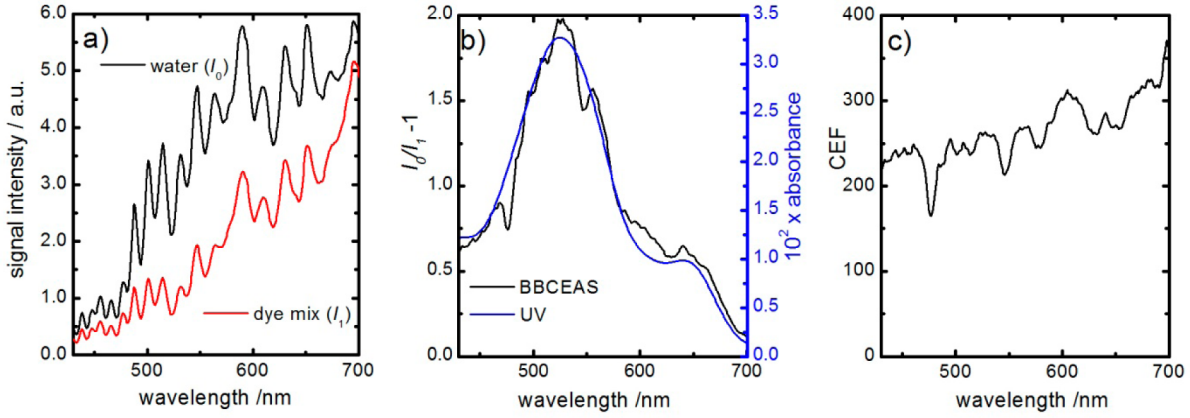

Figure 2. Determination of the spectrum of the cavity enhancement factor (CEF). (a) The intensity spectrum recorded with ultrapure water in the cell (I_0, black) and with a calibration mixture of 1 μM Acid Red and 1 μM Acid Green dye solution (I_1, red). (b) The BBCEAS observable ($I_0/I_1 - 1$), in black, compared with the UV–vis spectrum of the same dye mixture (in blue). (c) The CEF(λ) spectrum determined from the ratio of the spectra in (b), allowing for the difference in path-length.

E. Data Acquisition Protocol. CEAS does not provide absolute absorbance measurements directly. For this, calibration of the cavity enhancement factor is required (see eq 1) and various techniques exist for this purpose. Laurila et al. have demonstrated the use of phase-shift cavity ring-down spectroscopy in parallel with CEAS,[35] but in most cases calibration is achieved by recording the spectrum of a known absorber.[25,30]

At the start of each experimental run, the cavity is optimized and the spectrum of the cavity enhancement factor, CEF(λ), determined using a mixture of dyes whose combined absorbance spans the wavelength region of interest. First, the spectrum, denoted $I_0(\lambda)$, of light intensity transmitted by the optical cavity with ultrapure water in the sample cell is recorded. This constitutes the background signal and reflects (constant) per-pass mirror losses and absorption and scattering losses from the cell itself. The $I_0(\lambda)$ spectrum is highly structured (see Figure 2a), resulting from a combination of the intensity profile of the light source, the mirror reflectivity spectrum and the wavelength dependence of scattering from the fused silica cell. An $I_1(\lambda)$ spectrum is then recorded, under identical acquisition conditions except with a 1 μM Acid Red plus 1 μM Acid Green dye mixture in the cell. The CEF(λ) spectrum is then determined by comparison of the experimental observable, $(I_0(\lambda)/I_1(\lambda)) - 1$, with the absorption spectrum of the dye mixture recorded independently by conventional UV–vis spectroscopy. This CEF(λ) determination procedure is illustrated in Figure 2. Where required, the CEF(λ) spectrum can be used to convert subsequent BBCEAS measurements to absolute absorbance.

The CEF(λ) spectrum can change from day to day depending upon the exact cavity/cell alignment achieved, but typical values lie in the range 200–600, representing background per-pass losses of $(2 \times 10^{-3}) - (5 \times 10^{-3})$. The mirror reflectivity exceeds 0.9993 across the spectral range of interest, and thus it is clear that the per-pass losses are dominated by scattering/absorption losses in the cell itself. This somewhat tedious and imperfect calibration procedure is necessary only for establishing absolute absorbances. As will become clear, it is not required for fractional MFE measurements.

Following CEF(λ) determination, the cell is rinsed with ultrapure water and a new I_0 spectrum recorded. The cell is then filled with the solution to be studied. The transmitted intensity spectrum, $I_{GS}(\lambda)$, provides a measure of the ground state absorbance of the sample (using eq 1). When the sample is irradiated with the 405 nm photoexcitation laser, the spectrum of the transmitted light, $I_{h\nu}(\lambda)$, changes markedly as a result of the presence of new photogenerated species and the partial removal of ground state population (see Scheme 1). The change in absorbance, $\Delta A_{h\nu}(\lambda)$, arising from photoexcitation is determined as

$$\begin{aligned}\Delta A_{h\nu}(\lambda) &= A_{h\nu}(\lambda) - A_{GS}(\lambda) \\ &= \frac{1}{\ln 10 \times \mathrm{CEF}(\lambda)}\left[\left(\frac{I_0(\lambda)}{I_{h\nu}(\lambda)} - 1\right) - \left(\frac{I_0(\lambda)}{I_{GS}(\lambda)} - 1\right)\right] \\ &= \frac{1}{\ln 10 \times \mathrm{CEF}(\lambda)}\left[\frac{I_0(\lambda)(I_{GS}(\lambda) - I_{h\nu}(\lambda))}{I_{h\nu}(\lambda)I_{GS}(\lambda)}\right]\end{aligned} \quad (2)$$

MFEs are determined by recording the differential absorbance spectra in the presence and absence of externally applied homogeneous magnetic fields oriented mutually perpendicularly to the optical axis and the direction of sample flow. This comprises comparing the intensity of light transmitted by the cavity in the presence of a magnetic field, $I_B(\lambda)$, with that recorded at zero-field ($I_{h\nu}(\lambda)$). The B field, variable in the range -15 mT $\leq B \leq$ 15 mT (the field can be applied in opposing directions), is generated by passing controllable currents through the Helmholtz coils, the field in the region of the sample having been calibrated using a Hall probe. The field is applied for 100 ms intervals with the spectral acquisition timed to be 50 ms after the rising edge to permit (i) the field to rise to its final value (<10 ms) and (ii) the system to re-equilibrate at the new field. The B field measurements (taken at integer mT fields) were made in random order to minimize the effects of any systematic drift in the instrument performance. In order to minimize effects of drift in the spectrum of the SCR source, a B = 0 spectrum, $I_{h\nu}(\lambda)$, was recorded between different field measurements. We define the differential absorbance arising from the application of an external field as

dx.doi.org/10.1021/jp500732u | J. Phys. Chem. B 2014, 118, 4177–4184

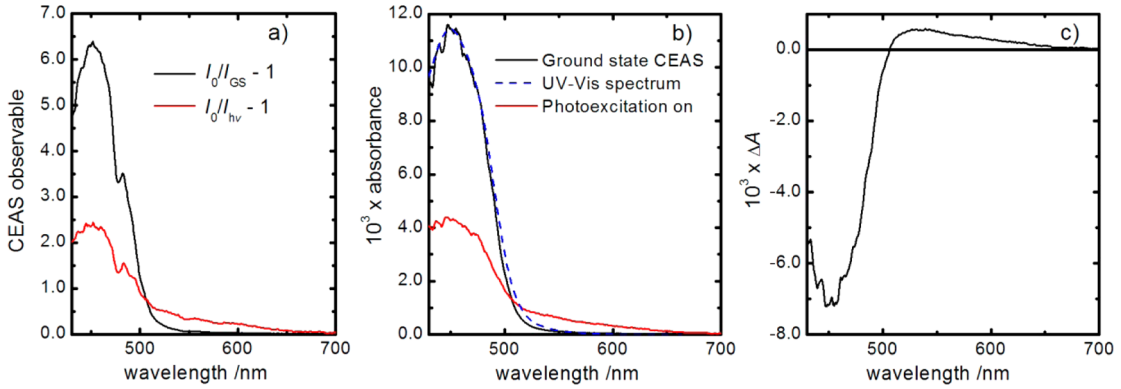

Figure 3. BBCEAS spectra (a) and (CEF(λ) corrected) absorbance spectra (b) of FMN | Lys solutions with (red) and without (black) photoexcitation at 405 nm. The CEF(λ) calibration is confirmed by the close match of the experimental ground-state spectrum with the scaled UV–vis spectrum (blue dashed line) also shown. Irradiation at 405 nm results in a decrease in absorbance in the FMN ground state absorption region (λ < 520 nm) and a concomitant increase in absorption for λ > 520 nm ascribed to production of the $FMN^{-\bullet}$ and $Trp(H)^{+\bullet}$ radicals. (c) The differential absorbance spectrum, $\Delta A(\lambda)$, arising from the photoexcitation at 405 nm.

$$\Delta\Delta A_B(\lambda) = A_B(\lambda) - A_{h\nu}(\lambda)$$

$$= \frac{1}{\ln 10 \times \mathrm{CEF}(\lambda)}\left[\left(\frac{I_0(\lambda)}{I_B(\lambda)} - 1\right) - \left(\frac{I_0(\lambda)}{I_{h\nu}(\lambda)} - 1\right)\right]$$

$$= \frac{1}{\ln 10 \times \mathrm{CEF}(\lambda)}\left[\frac{I_0(\lambda)(I_{h\nu}(\lambda) - I_B(\lambda))}{I_B(\lambda)I_{h\nu}(\lambda)}\right] \quad (3)$$

and, for comparison with other techniques, we define the fractional MFE at a particular field by convention as the ratio

$$\mathrm{MFE}(\lambda, B) = \frac{\Delta\Delta A_B(\lambda)}{\Delta A_{h\nu}(\lambda)} = \frac{I_{GS}(\lambda)(I_{h\nu}(\lambda) - I_B(\lambda))}{I_B(\lambda)(I_{GS}(\lambda) - I_{h\nu}(\lambda))} \quad (4)$$

Within this definition, it is clear that the magnitude of the detected MFE is independent of the cavity enhancement factor (and indeed the background spectrum, $I_0(\lambda)$).

III. RESULTS AND DISCUSSION

A. FMN | Lys. Figure 3 shows a typical ground-state absorbance spectrum for FMN | Lys and the change induced upon photoexcitation. Figure 3a depicts the CEAS observable, $(I_0(\lambda)/I(\lambda)) - 1$, in the presence, $(I_0(\lambda)/I_{h\nu}(\lambda)) - 1$, and absence, $(I_0(\lambda)/I_{GS}(\lambda)) - 1$, of the 405 nm excitation and Figure 3b depicts the absorbance spectra corrected for the CEF(λ) spectrum as described above. It is clear that the calibration removes several prominent dips in the spectral profile (e.g., at 480 nm). In the absence of photoexcitation, the spectrum recorded is simply the absorbance spectrum of the FMN | Lys solution and, following calibration, the spectrum matches very well the shape of the (scaled) conventional UV–vis spectrum (Figure 3b).

Photoexcitation at 405 nm results in a marked decrease in the sample absorbance at wavelengths λ < 520 nm, as a significant fraction (>50%) of the ground-state FMN molecules within the laser excitation volume are electronically excited. Simultaneously, at longer wavelengths, an increase in absorbance is observed reflecting the production of new species, notably the $FMN^{-\bullet}$ and $Trp(H)^{+\bullet}$ radicals. Figure 3c shows the differential absorbance spectrum, denoted $\Delta A(\lambda)$ (see eq 2), resulting from the photoexcitation. These are not strictly transient absorption measurements, but rather measurements of steady-state concentrations of species present in the sample cell. Within the photoexcitation region, species are continually cycling around the reactions shown in Scheme 1 or undergoing additional (slower) radical–radical recombination reactions. The larger change in the ground-state absorbance region reflects the higher extinction coefficient of the ground-state FMN species compared with that of the radical species.

The effect of an external magnetic field on the absorbance spectrum of the photoexcited FMN | Lys sample is shown in Figure 4. Figure 4a shows the full data represented as a $\Delta\Delta A(\lambda, B)$ surface plot, while Figure 4b shows the effect of a B = −15 mT field on the absorbance spectrum to illustrate both the high signal-to-noise achieved and the full spectral resolution.

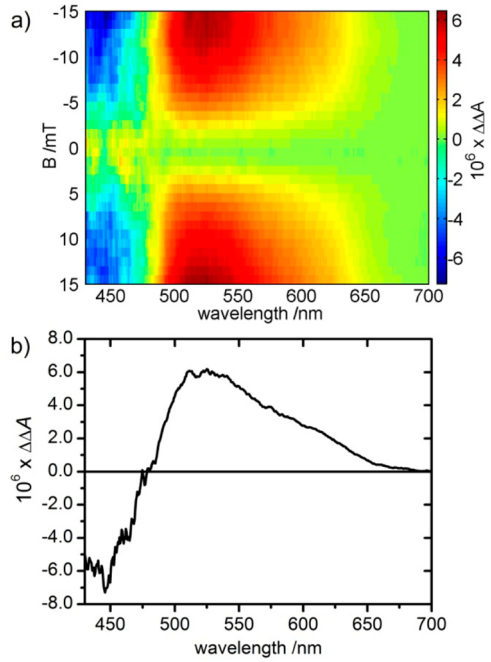

Figure 4. (a) Surface plot showing the effect, $\Delta\Delta A(\lambda)$, of an external magnetic field strength, B, on the absorbance spectrum of the FMN | Lys sample. (b) The $\Delta\Delta A(\lambda)$ spectrum at B = −15 mT.

The form of the $\Delta\Delta A(\lambda, B)$ data can be understood most easily in the region λ > 530 nm. The increase in absorbance in this region reflects the slightly increased population of $FMN^{-\bullet}$

dx.doi.org/10.1021/jp500732u | J. Phys. Chem. B 2014, 118, 4177–4184

and $Trp(H)^{+\bullet}$ radicals upon application of the field. This can be understood by reference to Scheme 1. As the magnetic field strength is increased, the T_+ and T_- states of the radical pair become energetically isolated from the S/T_0 manifold resulting in a decrease in singlet−triplet mixing efficiency. In the absence of significant spin relaxation, much of the (triplet-born) radical pair population thus becomes trapped in unreactive spin states. With radical recombination and singlet−triplet interconversion pathways unavailable to a proportion of the triplet radical pairs, the partners will finally diffuse apart increasing the free radical concentrations over those observed in the absence of a field.

The positive sign of the MFE is a clear indication of the triplet-born nature of the RP. The size of the MFE observed (which saturates at about 1% here) depends critically on the relative rates of the various RP decay processes, principally reverse electron transfer, the diffusive separation of the radicals, the strength of S−T mixing and the rate of spin relaxation. In the FMN | Lys reaction, the RP is formed by a bimolecular reaction. Reverse electron transfer (the principal route back to ground state products) is relatively inefficient and takes place only within the geminate RP. Diffusion competes effectively with this process leading to free radicals and resulting in the small MFE observed.

The observed effect of the magnetic field on the absorbance spectrum at shorter wavelengths is more complex as the absorption spectra of the FMN ground state and radical species overlap. An increase in the radical concentration must be accompanied by a decrease in the concentration of ground-state species. Hence, for λ < 520 nm, the $\Delta\Delta A(\lambda)$ spectrum represents the net effect of an increase in absorbance due to higher radical concentrations and a concomitant decrease in the ground-state FMN concentration. As a result, below 520 nm the form of the $\Delta\Delta A(\lambda)$ spectrum is markedly different to that for the $\Delta A(\lambda)$ in Figure 3c.

The effect induced by the external field is not large, manifesting itself as an absorbance change of $<6 \times 10^{-6}$ (around a 1% change) for the *B*-fields applied here ($|B| \leq$ 15 mT). Nevertheless, the sensitivity of the BBCEAS technique is such that these changes are recorded with high signal-to-noise. The minimum detectable absorbance change is different in different spectral regions due to the varying $CEF(\lambda)$ spectrum and the properties of the SCR source. However, averaged over a 10 nm spectral window, it can be as low as $(5 \pm 2) \times 10^{-8}$ (around 600 nm). When averaged over the radical absorption spectrum (500−650 nm) it can be as low as 2×10^{-8}. This represents a significant improvement on conventional transient absorption measurements as applied to MFE determination. A further improvement is the speed of data acquisition. The Fellgett advantage which this broadband technique provides means that a single complete data set (31 individual *B*-field measurements from −15 mT to +15 mT) takes less than 10 s to acquire. The full data set shown in Figure 4a represents a 500-experiment average, which takes ca. 80 min.

By convention, MFEs are reported as fractional changes in properties observed upon application of a magnetic field. In this case, this involves division of the surface plot in Figure 4a by the $\Delta A(\lambda)$ spectrum (Figure 3c) at all fields (as per eq 4). The result is shown in Figure 5a. One downside of this approach is the unreliability of data in the region close to 500 nm where $\Delta A(\lambda)$ passes through zero. For this reason, the data in the region 490−525 nm in Figure 5a are omitted. These MFE representations provide useful information, as any spectral region in which the MFE is constant indicates the presence of

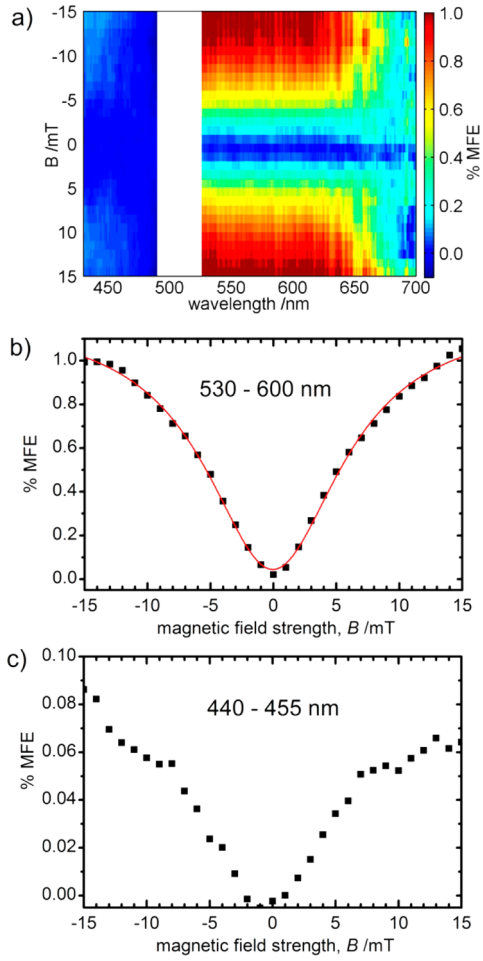

Figure 5. (a) %MFE(λ, *B*) surface plot. (b,c) MARY spectra averaged over (b) the radical absorbance region, 530−600 nm, and (c) the FMN ground state absorbance region, 440−455 nm. The red line in (b) shows a fit of the experimental data to a Lorentzian function with half width at maximum height = 6.6 mT.

species whose concentrations show identical field dependence (since no two species will have identical absorbance spectra). This is most clear in the region 530 nm < λ < 630 nm where the radical species are the only significant absorbers. Figure 5b,c shows magnetically altered reaction yield (MARY) spectra averaged over spectral regions dominated by radical absorption (530−600 nm) and FMN ground-state absorption (440−455 nm), respectively. The signal-to-noise is significantly better in the radical absorption region due to (i) the lack of interference from other absorbers and (ii) the fact that the SCR source provides more light, and is more stable in this region than further to the blue. Nevertheless, as expected, the overall shape of the MARY curves is similar in both regions. The shape can be characterized empirically by determination of the Weller $B_{1/2}$ value,[36] the magnetic field strength at which the MFE reaches half its maximum value. For this purpose, the MARY curve in the radical absorption region (Figure 5b) has been fitted to a Lorentzian function, shown on the figure in red. This yields a Lorentzian half-width of 6.6 ± 0.2 mT, markedly larger than the 3 mT predicted by theory,[36] but consistent with our earlier cavity ring-down measurements.[6]

B. FAD. Figure 6 shows the $\Delta A(\lambda)$ spectrum resulting from illumination of a 10 μM FAD solution at 405 nm. As expected, given the similarity of chromophores involved, the spectrum is

dx.doi.org/10.1021/jp500732u | J. Phys. Chem. B 2014, 118, 4177−4184

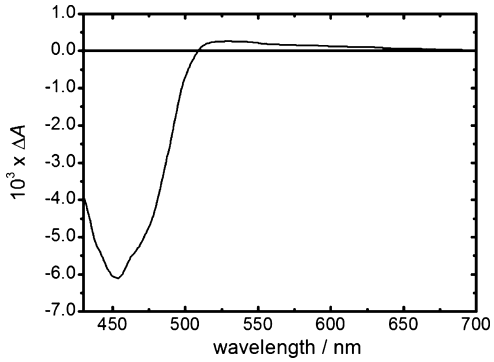

Figure 6. Differential absorbance spectrum, $\Delta A(\lambda)$ of a 10 μM FAD solution (pH 2.2) upon photoexcitation at 405 nm. The radical absorbance is clearly observed at wavelengths λ > 500 nm.

very like that shown in Figure 3c for FMN | Lys and exhibits clear ground-state bleaching for λ < 520 nm, as well as the presence of radical species (500 < λ < 650 nm).[15] Indeed, the spectra in Figure 6 and Figure 3c are so similar that they suggest that, rather than detecting $FH^{\bullet}$ directly (see Scheme 2), the absorbance observed is dominated by free radical species in the same way as in the FMN studies.[20] Free radical formation probably occurs by bimolecular reaction of the $^3F^*$ state (see Scheme 2). This interpretation is consistent with the short (~μs) RP lifetime observed in the FAD system, which results from efficient (*intra*molecular) electron/proton transfer. The continuous-wave nature of the present experiments makes them inherently more sensitive to longer-lived species rather than short-lived transient intermediates. Nevertheless, the equilibrium established as a result of combined proton and electron transfer between $^3F^*$-AH_2^+ and the $^3[FH^{\bullet}\ AH^{+\bullet}]$ radical pair confers magnetic field sensitivity on the free radical concentration (see Scheme 2).

The effect of the external B field on the $\Delta A(\lambda)$ spectrum is illustrated in both the surface plot of Figure 7a and the MARY curve in the radical absorbance region (averaged over 530 < λ < 600 nm, Figure 7b). The lower radical concentration compared with the FMN reaction is reflected in the reduced signal-to-noise achieved in the MARY curve. Nevertheless, clear $\Delta\Delta A(\lambda, B)$ changes of $<10^{-6}$ are observed in both the ground state and radical absorption regions. In the latter, this represents an unambiguous MFE of <1% recorded with high signal-to-noise.

IV. SUMMARY AND CONCLUSIONS

A new condensed-phase BBCEAS MFE spectrometer has been developed and applied to the study of two chemical systems which, in their photochemical reaction schemes, are models for magnetosensitivity in cryptochromes. The instrument couples light from a supercontinuum white light source with a simple optical cavity formed by two broadband-coated mirrors to provide full visible spectral coverage (425−750 nm). At the center of the cavity lies a 1 mm path-length sample cuvette surrounded by Helmholtz coils which allow the application of external magnetic fields. The optical properties of the cavity have been characterized using known absorbers, and even without specific cuvette coatings, a cavity enhancement factor of >200 throughout the visible region is achieved.

In the first application of the new spectrometer, continuous-wave BBCEAS has been used to study the effects of externally applied magnetic fields on reactions of FMN and FAD proceeding via photogenerated spin-correlated radical pairs.

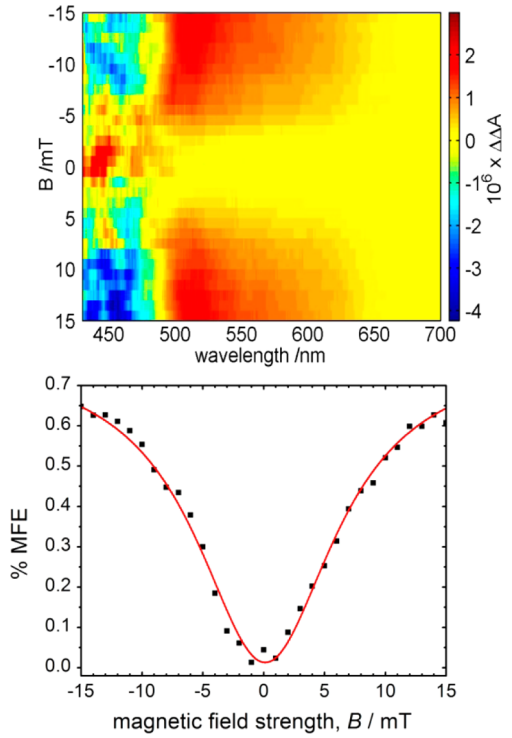

Figure 7. (a) Surface plot of the effect, $\Delta\Delta A(\lambda)$, of an external magnetic field, strength B, on the absorbance spectrum of the FAD sample. (b) The MARY (or %MFE) spectrum averaged over the radical absorbance region (530 < λ < 600 nm). The fit shows a Lorentzian function with half width at maximum height, 7.0 mT.

Full, two-dimensional MFE(B, λ) data provide information simultaneously on different absorbers present in these complex systems with unprecedented sensitivity. In favorable spectral regions, minimum detectable absorbances of $<1 \times 10^{-7}$ can be measured permitting the detection of MFEs $<10^{-4}$. The combination of this level of sensitivity together with the broadband coverage and the small cuvette volume (ca. 50 μL, of which <5 μL is actually sampled during an individual experiment) offer considerable promise in the detection of MFEs in real biological samples.

AUTHOR INFORMATION

Corresponding Authors

*E-mail: christiane.timmel@chem.ox.ac.uk.

*E-mail: stuart.mackenzie@chem.ox.ac.uk, tel. 44 (0) 1865 275156.

Author Contributions

S. R. T. N., J. L., and D. M. W. S. contributed equally to various stages of the development of the instruments and the protocols for the recording of the data presented. J. S. was responsible for the data acquisition software.

Notes

The authors declare no competing financial interest.

ACKNOWLEDGMENTS

The authors are grateful for the financial support of this work from DARPA (QuBE: N66001-10-1-4061), the Royal Society, and the EMF Biological Research Trust. We are grateful to the staff of the mechanical and electronic workshops in the Oxford Chemistry Department, without whom none of this work would have been possible.

REFERENCES

(1) Ritz, T.; Adem, S.; Schulten, K. A Model for Photoreceptor-Based Magnetoreception in Birds. *Biophys. J.* **2000**, *78*, 707−718.

(2) Kaptein, R.; Oosterhoff, J. L. Chemically Induced Dynamic Nuclear Polarization II - (Relation with Anomalous ESR Spectra). *Chem. Phys. Lett.* **1969**, *4*, 195−197.

(3) Closs, G. L. A Mechanism Explaining Nuclear Spin Polarizations in Radical Combination Reactions. *J. Am. Chem. Soc.* **1969**, *91*, 4552−4554.

(4) Mouritsen, H.; Hore, P. J. The Magnetic Retina: Light-Dependent and Trigeminal Magnetoreception in Migratory Birds. *Curr. Opin. Neurobiol.* **2012**, *22*, 343−352.

(5) Maeda, K.; Robinson, A. J.; Henbest, K. B.; Hogben, H. J.; Biskup, T.; Ahmad, M.; Schleicher, E.; Weber, S.; Timmel, C. R.; Hore, P. J. Magnetically Sensitive Light-Induced Reactions in Cryptochrome are Consistent with its Proposed Role as a Magnetoreceptor. *Proc. Natl. Acad. Sci. U. S. A.* **2012**, *109*, 4774−4779.

(6) Maeda, K.; Neil, S. R. T.; Henbest, K. B.; Weber, S.; Schleicher, E.; Hore, P. J.; Mackenzie, S. R.; Timmel, C. R. Following Radical Pair Reactions in Solution: A Step Change in Sensitivity Using Cavity Ring-Down Detection. *J. Am. Chem. Soc.* **2011**, *133*, 17807−17815.

(7) Steiner, U. E.; Ulrich, T. Magnetic Field Effects in Chemical Kinetics and Related Phenomena. *Chem. Rev.* **1989**, *89*, 51−147.

(8) Timmel, C. R.; Henbest, K. B. A Study of Spin Chemistry in Weak Magnetic Fields. *Philos. Trans. R. Soc. Lond., Ser. A* **2004**, *362*, 2573−2589.

(9) Woodward, J. R. Radical Pairs in Solution. *Prog. React. Kinet. Mech.* **2002**, *27*, 165−207.

(10) Evans, E. W.; Dodson, C. A.; Maeda, K.; Biskup, T.; Wedge, C. J.; Timmel, C. R. Magnetic Field Effects in Flavoproteins and Related Systems. *Interface Focus* **2013**, *3*, 20130037.

(11) Maeda, K.; Henbest, K. B.; Cintolesi, F.; Kuprov, I.; Rodgers, C. T.; Liddell, P. A.; Gust, D.; Timmel, C. R.; Hore, P. J. Chemical Compass Model of Avian Magnetoreception. *Nature* **2008**, *453*, 387−390.

(12) Neil, S. R. T.; Maeda, K.; Henbest, K. B.; Goez, M.; Hemmens, R.; Timmel, C. R.; Mackenzie, S. R. Cavity Enhanced Detection Methods for Probing the Dynamics of Spin Correlated Radical Pairs in Solution. *Mol. Phys.* **2010**, *108*, 993−1003.

(13) Wheeler, M. D.; Newman, S. M.; Orr-Ewing, A. J.; Ashfold, M. N. R. Cavity Ring-Down Spectroscopy. *J. Chem. Soc., Faraday Trans* **1998**, *94*, 337−351.

(14) Berden, G.; Peeters, R.; Meijer, G. Cavity Ring-Down Spectroscopy: Experimental Schemes and Applications. *Int. Rev. Phys. Chem.* **2000**, *19*, 565−607.

(15) Liu, B.; Liu, H. T.; Zhong, D. P.; Lin, C. T. Searching for a Photocycle of the Cryptochrome Photoreceptors. *Curr. Opin. Plant Biol.* **2010**, *13*, 578−586.

(16) Miura, T.; Maeda, K.; Arai, T. Effect of Coulomb Interaction on the Dynamics of the Radical Pair in the System of Flavin Mononucleotide and Hen Egg-White Lysozyme (HEWL) Studied by a Magnetic Field Effect. *J. Phys. Chem. B* **2003**, *107*, 6474−6478.

(17) Horiuchi, M.; Maeda, K.; Arai, T. Magnetic Field Effect on Electron Transfer Reactions of Flavin Derivatives Associated with Micelles. *Appl. Magn. Reson.* **2003**, *23*, 309−318.

(18) Hore, P. J. Are Biochemical Reactions Affected by Weak Magnetic Fields? *Proc. Natl. Acad. Sci. U. S. A.* **2012**, *109*, 1357−1358.

(19) Murakami, M.; Maeda, K.; Arai, T. Structure and Kinetics of the Intermediate Biradicals Generated from Intramolecular Electron Transfer Reaction of FAD Studied by an Action Spectrum of the Magnetic Field Effect. *Chem. Phys. Lett.* **2002**, *362*, 123−129.

(20) Murakami, M.; Maeda, K.; Arai, T. Dynamics of Intramolecular Electron Transfer Reaction of FAD Studied by Magnetic Field Effects on Transient Absorption Spectra. *J. Phys. Chem. A* **2005**, *109*, 5793−5800.

(21) Stob, S.; Kemmink, J.; Kaptein, R. Intramolecular Electron-Transfer in Flavin Adenine-Dinucleotide - Photochemically Induced Dynamic Nuclear-Polarization Study at High and Low Magnetic-Fields. *J. Am. Chem. Soc.* **1989**, *111*, 7036−7042.

(22) Engeln, R.; Berden, G.; Peeters, R.; Meijer, G. Cavity Enhanced Absorption and Cavity Enhanced Magnetic Rotation Spectroscopy. *Rev. Sci. Instrum.* **1998**, *69*, 3763−3769.

(23) Ouyang, B.; Jones, R. L. Understanding the Sensitivity of Cavity-Enhanced Absorption Spectroscopy: Pathlength Enhancement Versus Noise Suppression. *Appl. Phys. B: Laser Opt.* **2012**, *109*, 581−591.

(24) Fiedler, S. E.; Hese, A.; Ruth, A. A. Incoherent Broad-Band Cavity-Enhanced Absorption Spectroscopy of Liquids. *Rev. Sci. Instrum.* **2005**, *76*, 023107.

(25) Islam, M.; Seetohul, L. N.; Ali, Z. Liquid-Phase Broadband Cavity-Enhanced Absorption Spectroscopy Measurements in a 2 mm Cuvette. *Appl. Spectrosc.* **2007**, *61*, 649−658.

(26) Seetohul, L. N.; Ali, Z.; Islam, M. Broadband Cavity Enhanced Absorption Spectroscopy as a Detector for HPLC. *Anal. Chem.* **2009**, *81*, 4106−4112.

(27) Seetohul, L. N.; Ali, Z.; Islam, M. Liquid-Phase Broadband Cavity Enhanced Absorption Spectroscopy (BBCEAS) Studies in a 20 cm Cell. *Analyst* **2009**, *134*, 1887−1895.

(28) Qu, Z.; Engstrom, J.; Wong, D.; Islam, M.; Kaminski, C. F. High Sensitivity Liquid Phase Measurements using Broadband Cavity Enhanced Absorption Spectroscopy (BBCEAS) Featuring a Low Cost Webcam Based Prism Spectrometer. *Analyst* **2013**, *138*, 6372−6379.

(29) Kiwanuka, S. S.; Laurila, T.; Kaminski, C. F. Sensitive Method for the Kinetic Measurement of Trace Species in Liquids Using Cavity Enhanced Absorption Spectroscopy with Broad Bandwidth Supercontinuum Radiation. *Anal. Chem.* **2010**, *82*, 7498−7501.

(30) Ruth, A. A.; Lynch, K. T. Incoherent Broadband Cavity-Enhanced Total Internal Reflection Spectroscopy of Surface-Adsorbed Metallo-Porphyrins. *Phys. Chem. Chem. Phys.* **2008**, *10*, 7098−7108.

(31) Schnippering, M.; Neil, S. R. T.; Mackenzie, S. R.; Unwin, P. R. Evanescent Wave Cavity-Based Spectroscopic Techniques as Probes of Interfacial Processes. *Chem. Soc. Rev.* **2011**, *40*, 207−220.

(32) Schnippering, M.; Unwin, P. R.; Hult, J.; Laurila, T.; Kaminski, C. F.; Langridge, J. M.; Jones, R. L.; Mazurenka, M.; Mackenzie, S. R. Evanescent Wave Broadband Cavity Enhanced Absorption Spectroscopy using Supercontinuum Radiation: A New Probe of Electrochemical Processes. *Electrochem. Commun.* **2008**, *10*, 1827−1830.

(33) van der Sneppen, L.; Hancock, G.; Kaminski, C.; Laurila, T.; Mackenzie, S. R.; Neil, S. R. T.; Peverall, R.; Ritchie, G. A. D.; Schnippering, M.; Unwin, P. R. Following Interfacial Kinetics in Real Time Using Broadband Evanescent Wave Cavity-Enhanced Absorption Spectroscopy: A Comparison of Light-Emitting Diodes and Supercontinuum Sources. *Analyst* **2010**, *135*, 133−139.

(34) Langridge, J. M.; Laurila, T.; Watt, R. S.; Jones, R. L.; Kaminski, C. F.; Hult, J. Cavity enhanced absorption spectroscopy of multiple trace gas species using a supercontinuum radiation source. *Opt. Express* **2008**, *16*, 10178−10188.

(35) Laurila, T.; Burns, I. S.; Hult, J.; Miller, J. H.; Kaminski, C. F. A calibration method for broad-bandwidth cavity enhanced absorption spectroscopy performed with supercontinuum radiation. *Appl. Phys. B: Laser Opt.* **2011**, *102*, 271−278.

(36) Weller, A.; Nolting, F.; Staerk, H. A quantitative interpretation of the magnetic field effect on hyperfine coupling-induced triplet fromation from radical ion pairs. *Chem. Phys. Lett.* **1983**, *96*, 24−27.